Atmospheric and oceanic excitation of length-of-day variations during 1980–2000

Richard S. Gross, Ichiro Fukumori, and Dimitris Menemenlis
Jet Propulsion Laboratory, California Institute of Technology, Pasadena, California, USA

Pascal Gegout
Institut de Physique du Globe, Strasbourg, France

Received 5 February 2003; revised 1 October 2003; accepted 14 October 2003; published 15 January 2004.

[1] Although nontidal changes in the Earth's length-of-day on timescales of a few days to a few years are primarily caused by changes in the angular momentum of the zonal winds, other processes can be expected to cause the length-of-day to change as well. Here the relative contribution of upper atmospheric winds, surface pressure, oceanic currents, and ocean-bottom pressure to changing the length-of-day during 1980–2000 is evaluated using estimates of atmospheric angular momentum from the National Centers for Environmental Prediction/National Center for Atmospheric Research reanalysis project, estimates of the angular momentum of the zonal winds in the upper atmosphere from the United Kingdom Meteorological Office, and estimates of oceanic angular momentum from the Estimating the Circulation and Climate of the Ocean consortium's simulation of the general circulation of the oceans. On intraseasonal timescales, atmospheric surface pressure, oceanic currents, and ocean-bottom pressure are found to be about equally important in causing the length-of-day to change, while upper atmospheric winds are found to be less important than these mechanisms. On seasonal timescales, the upper atmospheric winds are more important than the sum of currents and bottom pressure in causing the length-of-day to change and, except at the annual frequency, are even more important than surface pressure changes. On interannual timescales, oceanic currents and ocean-bottom pressure are found to be only marginally effective in causing the length-of-day to change. *INDEX TERMS:* 1223 Geodesy and Gravity: Ocean/Earth/atmosphere interactions (3339); 1239 Geodesy and Gravity: Rotational variations; 3319 Meteorology and Atmospheric Dynamics: General circulation; 4532 Oceanography: Physical: General circulation; *KEYWORDS:* Earth rotation, length-of-day, oceanic angular momentum

Citation: Gross, R. S., I. Fukumori, D. Menemenlis, and P. Gegout (2004), Atmospheric and oceanic excitation of length-of-day variations during 1980–2000, *J. Geophys. Res.*, *109*, B01406, doi:10.1029/2003JB002432.

1. Introduction

[2] The Earth's rate of rotation, and hence the length of the day, is not constant but varies by up to a millisecond-per-day on all observable timescales from subdaily to decadal and longer (for reviews see, e.g., *Munk and MacDonald* [1960], *Lambeck* [1980, 1988], and *Eubanks*, 1993]). Such observed changes in the Earth's rate of rotation are caused by a wide variety of processes, both internal and external to the solid body of the Earth. Tidal forces due to the gravitational attraction of the Sun, Moon, and planets cause harmonic changes in the Earth's rotation having periods ranging from 12 hours to 18.6 years. By exchanging angular momentum with the solid Earth, changes in the east-west, or zonal, component of the winds caused by changes in the land-ocean temperature contrast and in the pole-to-equator temperature gradient cause the Earth's rate of rotation to change. Changes in the mass distribution of the atmosphere, which manifest themselves as changes in surface pressure, also change the Earth's rotation by changing its inertia tensor. Recently, the advent of accurate models of the general circulation of the oceans has allowed the effect of the oceans on the length of the day to be evaluated.

[3] Earlier investigations of nontidal effects of the oceans on the length-of-day (LOD) focused on seasonal changes due to their relatively large amplitude [*Brosche and Sündermann*, 1985; *Brosche et al.*, 1990; *Frische and Sündermann*, 1990; *Dickey et al.*, 1993]. Nonseasonal oceanic effects have lately been studied using both TOPEX/Poseidon sea surface height measurements that have been corrected for steric effects [*Chen et al.*, 2000b] and barotropic [*Ponte*, 1997; *Ponte and Ali*, 2002] and baroclinic [*Brosche et al.*, 1997; *Segschneider and Sündermann*, 1997; *Marcus et al.*, 1998; *Johnson et al.*, 1999; *Ponte and Stammer*, 2000; *Gross*, 2003a] models of the oceans' circulation.

[4] The Estimating the Circulation and Climate of the Oceans (ECCO) consortium [*Stammer et al.*, 2002] has

0148-0227/04/2003JB002432$09.00

recently simulated the oceans' circulation since 1980. In a companion paper, *Gross et al.* [2003] have used the results of the ECCO simulation to examine the effects of the oceans on the nonaxial components of the Earth's rotation vector. Here the ECCO simulation results are used to evaluate the effects of the oceans on the axial component.

[5] The contribution of changes in oceanic currents and bottom pressure to changing the Earth's length-of-day will be compared to that of atmospheric winds and surface pressure on intraseasonal, seasonal, and interannual timescales. Although atmospheric winds are the dominant cause of LOD changes on these timescales, it will be shown that closer agreement with the observations is obtained when the effects of oceanic current and bottom pressure changes, as estimated by the ECCO simulation during 1980–2000, are included with those of winds and surface pressure changes.

2. Length-of-Day Variations

[6] The rotational rate of the solid Earth, and hence the length of the day, changes due to the action of torques acting on the solid Earth and to changes in the mass distribution of the solid Earth. Observed changes in the length-of-day can be studied using the principle of conservation of angular momentum which, in a rotating, body-fixed terrestrial reference frame, is given by

$$\frac{\partial \mathbf{L}}{\partial t} + \boldsymbol{\omega} \times \mathbf{L} = \boldsymbol{\tau}, \tag{1}$$

where $\boldsymbol{\omega}$ is the Earth's rotation vector, $\mathbf{L}$ is its angular momentum vector, and $\boldsymbol{\tau}$ are the torques acting on the Earth. In general, the angular momentum vector $\mathbf{L}(t)$ can be written as the sum of a term $\mathbf{h}(t)$ due to motion relative to the rotating reference frame and of a term due to changes in the inertia tensor $\mathbf{I}(t)$ of the body caused by changes in the distribution of mass,

$$\mathbf{L} = \mathbf{I} \cdot \boldsymbol{\omega} + \mathbf{h}. \tag{2}$$

[7] The Earth's rotation deviates only slightly from a state of uniform rotation, the deviation being a few parts in 10^8 in speed, corresponding to changes of a few milliseconds (ms) in the length of the day, and about a part in 10^6 in the orientation of the rotation axis relative to the crust of the Earth, corresponding to a variation of several hundred milliarcseconds (mas) in polar motion. Such small deviations in rotation can be studied by linearizing equations (1) and (2). Let the Earth initially be uniformly rotating about its figure axis and orient the rotating, body-fixed terrestrial reference frame so that its z axis is aligned with the figure axis. Under a small perturbation to this initial state, the relative angular momentum $\mathbf{h}$ will be perturbed to $\mathbf{h} + \Delta\mathbf{h}$, the inertia tensor $\mathbf{I}$ will be perturbed to $\mathbf{I} + \Delta\mathbf{I}$, and the angular velocity vector $\boldsymbol{\omega}$ will be perturbed to $\boldsymbol{\omega} + \Delta\boldsymbol{\omega}$ where

$$\boldsymbol{\omega} + \Delta\boldsymbol{\omega} = \Omega \left[m_x(t), m_y(t), 1 + m_z(t)\right]^{\mathrm{T}}, \tag{3}$$

where Ω is the mean angular velocity of the Earth and the Ωm_i are the elements of the perturbed rotation vector. Keeping terms to first order in perturbed quantities, the axial component of equation (1) can be written in the absence of external torques as [e.g., *Munk and MacDonald*, 1960; *Wahr*, 1982; *Barnes et al.*, 1983],

$$\Delta\Lambda(t) = \frac{\Lambda_o}{C_m \Omega}\left[\Delta h_z(t) + 0.756\Omega \Delta I_{zz}(t)\right], \tag{4}$$

where the change $\Delta\Lambda(t)$ in the length of the day is related to $m_z(t)$ by $\Delta\Lambda(t)/\Lambda_o = -m_z(t)$, Λ_o is the nominal length-of-day of 86,400 s, C_m is the polar moment of inertia of the Earth's crust and mantle, and the factor of 0.756 accounts for the yielding of the crust and mantle to imposed surface loads.

[8] In this study, equation (4), which is called here the length-of-day equation, will be used to compare observed length-of-day changes with modeled variations computed using the products of atmospheric and oceanic general circulation models. Modeled length-of-day variations will be computed from modeled changes in the angular momentum of atmospheric winds and surface pressure and oceanic currents and bottom pressure. The relative importance of these processes to changing the length of the day will be assessed by comparing the modeled with the observed variations in both the time and frequency domains. Throughout this paper, statements about the contribution of some process to changing the length-of-day are based on the angular momentum associated with that process and not on the torques by which the angular momentum is transferred to the solid Earth. In particular, statements about the contribution of atmospheric surface and oceanic bottom pressure variations to changing the length of the day are based upon the angular momentum due to mass redistribution within the atmosphere and oceans, which manifests itself as changes in surface and bottom pressure, respectively, and not upon the torque exerted on the solid Earth by differential pressure forces.

3. Data Sets

3.1. Observed Length-of-Day Variations

[9] The daily version of the COMB2000 observed length-of-day series [*Gross*, 2001a] is used in this study. This series is derived from a combination of Universal Time measurements taken by the techniques of optical astrometry, lunar and satellite laser ranging, and very long baseline interferometry. Besides estimating Universal Time, the Kalman filter used to combine the measurements also estimates its time rate-of-change and hence the length-of-day [*Gross et al.*, 1998]. The COMB2000 length-of-day series spans January 20, 1962, to January 6, 2001, at daily intervals.

[10] Prior to investigating the effects of the atmosphere and oceans on the length-of-day, other sources of LOD variations that can be accurately modeled should be removed from the observations. Thus the model of *Yoder et al.* [1981] for the long-period solid Earth tides and the model of *Kantha et al.* [1998] for the long-period ocean tides have been used to remove these effects from the length-of-day observations. The resulting observed nontidal LOD variations during 1980–2000 are shown in Figure 1. The mean value of these observed LOD variations will be removed prior to comparing them to the modeled variations in order to isolate the changes in the LOD that may be

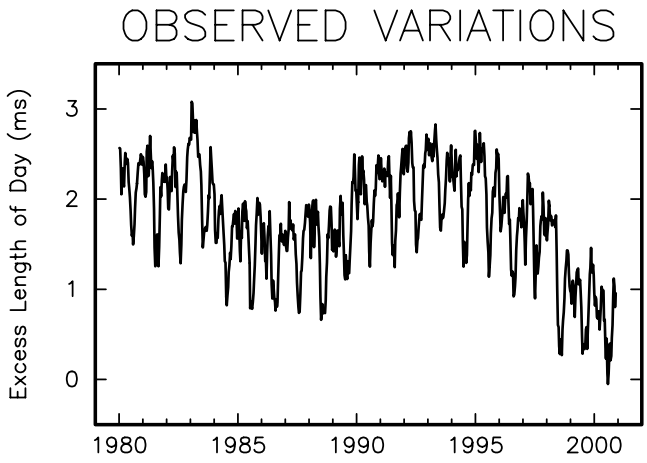

Figure 1. The COMB2000 series of observed length-of-day variations during 1980–2000 from which tidal effects have been removed. For purposes of clarity of display, 10-day averages of the observed daily values are shown. The mean has not been removed from the displayed values which show the amount by which the observed length-of-day exceeds a nominal length of exactly 86,400 s.

caused by changes in the modeled atmospheric and oceanic angular momentum.

3.2. Oceanic Angular Momentum

[11] The oceanic angular momentum (OAM) series used in this study, which is the same as that used in the companion paper on the effect of the atmosphere and oceans on the Earth's wobbles [*Gross et al.*, 2003], has been computed from the results of the simulation study done at JPL as part of their participation in the Estimating the Circulation and Climate of the Ocean (ECCO) consortium [*Stammer et al.*, 2002]. The ocean model used in this simulation study is based on the MIT ocean general circulation model [*Marshall et al.*, 1997a, 1997b] and has realistic boundaries and bottom topography, 46 levels ranging in thickness from 10 m at the surface to 400 m at depth using height as the vertical coordinate, and spans the globe between 73.5°S to 73.5°N latitude with a latitudinal grid-spacing ranging from 1/3° at the equator to 1° at high latitudes and a longitudinal grid-spacing of 1°. The simulation run is initialized with climatological temperature and salinity distributions [*Levitus and Boyer*, 1994; *Levitus et al.*, 1994] and is spun-up from rest for 10 years using climatological forcing fields from the Comprehensive Ocean-Atmosphere Data Set (COADS). The model is subsequently forced with twice daily wind stress and daily surface heat flux and evaporation-precipitation fields from the National Centers for Environmental Prediction/National Center for Atmospheric Research (NCEP/NCAR) reanalysis project [*Kalnay et al.*, 1996].

[12] Atmospheric surface pressure was not used to force the ocean model. At periods greater than a few days, the predominant response of the oceans to surface pressure forcing is a simple static response like that of an inverted barometer [*Wunsch and Stammer*, 1997]. This static response has been taken into account here during the computation of the angular momentum associated with atmospheric surface pressure changes (see section 3.3). The dynamical response of the oceans to surface pressure forcing at periods greater than a few days has been shown to be negligibly smaller than the response caused by wind stress forcing [e.g., *Frankignoul and Müller*, 1979; *Willebrand et al.*, 1980; *Ponte*, 1993, 1994]. However, at periods less than a few days, the dynamical response of the oceans to pressure forcing is comparable to that of wind stress forcing. Neglecting the dynamical response of the oceans to pressure forcing can thus be expected to adversely affect the agreement of the modeled oceanic angular momentum with the observed LOD variations at periods less than a few days but to have little impact at longer periods.

[13] Since the version of the MIT ocean general circulation model (OGCM) used in the simulation study is formulated under the Boussinesq approximation [*Marshall et al.*, 1997a, 1997b], it conserves volume rather than mass. Artificial mass variations can be introduced into Boussinesq models because of the applied surface heat and salt fluxes. For example, the changing applied heat flux will change the density, which, since volume is conserved, will artificially change the mass of the modeled oceans. If left uncorrected, this artificial mass change will cause artificial changes to the ocean-bottom pressure and hence to the angular momentum associated with ocean-bottom pressure variations. Following the suggestion of *Greatbatch* [1994], mass conservation is commonly imposed a posteriori on Boussinesq ocean models by adding to the sea surface a spatially uniform layer of just the right fluctuating thickness even though the correction should, in general, be spatially heterogeneous. Although not perfect [*Greatbatch et al.*, 2001; *Huang and Jin*, 2002], this approach of adding a spatially uniform layer has been shown to be effective in correcting the sea surface height fields of Boussinesq ocean models [*Mellor and Ezer*, 1995; *Dukowicz*, 1997] and has been widely used to correct the angular momentum [e.g., *Bryan*, 1997; *Marcus et al.*, 1998; *Ponte and Stammer*, 2000; *Gross et al.*, 2003] and bottom pressure fields [*Ponte*, 1999] of such models. It has been used here to correct the OAM pressure term for the effects of artificial mass variations in the MIT ocean model by computing the effect on the angular momentum of the spatially uniform mass-conserving layer. It is therefore assumed here that the errors introduced by using a spatially uniform mass-conserving layer rather than a spatially heterogeneous one are negligibly small.

[14] The axial component $L_{c,z}(t)$ of the angular momentum of the oceanic currents has been computed by integrating the eastward zonal currents $u(\mathbf{r}, t)$ throughout the volume V_o of the modeled oceans,

$$L_{c,z}(t) = \int_{V_o} \rho(\mathbf{r}, t) r \cos\phi u(\mathbf{r}, t) dV, \tag{5}$$

where ϕ is North latitude and $\rho(\mathbf{r}, t)$ is the density of some mass element located at position $\mathbf{r}$. The axial component $L_{p,z}(t)$ of the angular momentum due to changes in the mass distribution of the oceans, or, equivalently, due to changes in ocean-bottom pressure, has been computed by integrating the time-dependent density field throughout the volume of the modeled oceans,

$$L_{p,z}(t) = \Omega \int_{V_o} \rho(\mathbf{r}, t) r^2 \cos^2\phi dV, \tag{6}$$

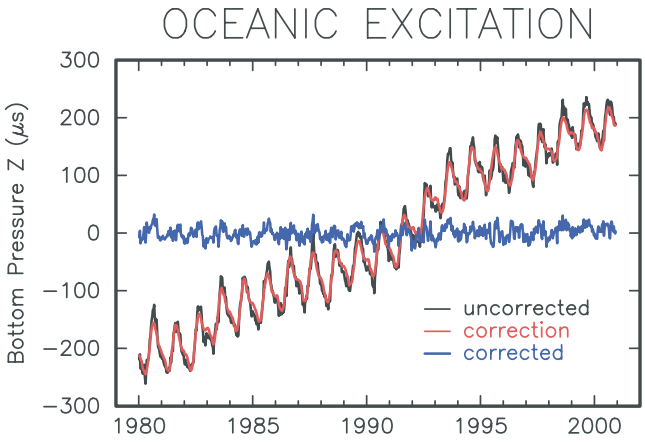

Figure 2. Axial component of the angular momentum associated with ocean-bottom pressure variations, in equivalent length-of-day units, both before (diagonal black curve) and after (horizontal blue curve) correcting it for the effects of artificial mass variations due to the use of the Boussinesq approximation in the MIT ocean model. The correction that has been applied to the pressure OAM term is shown by the smoother red curve overlying the uncorrected values shown in black. For purposes of clarity of display, 10-day averages of the hourly OAM values are shown. The mean has been removed from all series.

where Ω is the mean angular velocity of the Earth. When using equations (5) and (6) to calculate the axial OAM, the effects of both enforcing mass conservation and of changes in sea surface height have been included. Note that in equation (6) the total density of seawater has been used rather than the deviation of the density from some mean value. Thus the resulting angular momentum values include a nonzero mean due to the mean mass distribution, or mean moment of inertia, of the oceans. In order to isolate the fluctuations about the mean that causes the length-of-day to change, the mean value has been removed from this and the other angular momentum series just as it has been removed from the length-of-day observations.

[15] The angular momentum of the oceans has been computed at hourly intervals even though the ocean model is forced with twice daily wind stress and daily surface buoyancy fluxes. This was done in order to capture changes in the modeled oceanic angular momentum that can be expected to occur between the epochs of the surface forcing due to the dynamical response of the oceans to the forcing. The modeled oceanic angular momentum values, which span 1980–2000, were converted to equivalent length-of-day variations using equation (4) with values of 7.292115×10^{-5} rad/s for Ω and 7.1242×10^{37} kg-m^2 for C_m, and with $\Delta h_z(t) = L_{c,z}(t)$ and $\Omega\, \Delta I_{zz}(t) = L_{p,z}(t)$. In order to match the temporal resolution of the observed LOD variations, daily averages of the hourly values were computed by summing 25 consecutive values using weights of 1/48, 1/24, 1/24 . . ., 1/24, 1/24, 1/48.

[16] Figure 2 shows the axial component of the angular momentum associated with ocean-bottom pressure variations, in equivalent length-of-day units, both before and after correcting it for the effects of artificial mass variations within the MIT ocean model. The uncorrected series is given by the black curve with the correction that must be applied to it being given by the smoother red curve overlying it. The corrected series is the horizontal blue curve. As can be seen, and unlike the nonaxial components [see *Gross et al.*, 2003, Figure 1], the correction that must be applied to the axial component is nearly as large as the uncorrected values themselves. It is therefore important that the values for the correction be accurately computed since any errors in the computed correction will be fully transmitted to the corrected series. In particular, when computing the correction, it is important to use the same land-ocean mask that is used within the ocean model. Otherwise, the surface extent of the mass-conserving layer will be erroneous, with the effect of this error being fully propagated to the corrected values. Here the same land-ocean mask that was used in the ECCO simulation study has been used when correcting the axial component of the pressure OAM term.

[17] The corrected angular momentum associated with ocean-bottom pressure variations is reproduced in Figure 3d, with Figure 3c showing the angular momentum associated with oceanic currents. The mean value has been removed from these series in order to isolate the variations about the mean that cause the length-of-day to vary. As can be seen, the axial angular momenta due to oceanic currents and bottom pressure changes exhibit variability of similar magnitude.

3.3. Atmospheric Angular Momentum

[18] The atmospheric angular momentum (AAM) series used in this study, which is the same as that used in the companion paper on the effect of the atmosphere and oceans on the Earth's wobbles [*Gross et al.*, 2003], is that determined from the products of the NCEP/NCAR reanalysis project and have been obtained from the International Earth Rotation Service (IERS) Special Bureau for the Atmosphere (SBA) [*Salstein et al.*, 1993]. Both the angular momentum of the zonal winds, computed by integrating them from the surface to the top of the model at 10 hPa [*Salstein and Rosen*, 1997], and the angular momentum associated with surface pressure variations, computed by assuming that the oceans respond as an inverted barometer to the imposed surface pressure variations, are used here.

[19] The NCEP/NCAR reanalysis AAM series available from the IERS SBA spans January 1, 1948, to the present at 6-hour intervals. In order to match the temporal resolution of the observed COMB2000 length-of-day series, daily averages of the AAM were formed by summing five consecutive values using weights of 1/8, 1/4, 1/4, 1/4, 1/8. The resulting daily AAM series during 1980–2000 are shown in Figure 3, with that due to the zonal winds shown in Figure 3a and that associated with surface pressure variations shown in Figure 3b. The mean value has also been removed from these series in order to again isolate the variations about the mean that cause the length-of-day to vary. As can be seen, changes in the axial component of AAM associated with surface pressure variations are about an order of magnitude smaller than those associated with changes in the zonal winds, but are about 3 times larger than those due to either oceanic current or bottom pressure variations.

4. Seasonal Variations

[20] Numerous studies have shown that the observed annual and semiannual variations in the length-of-day are

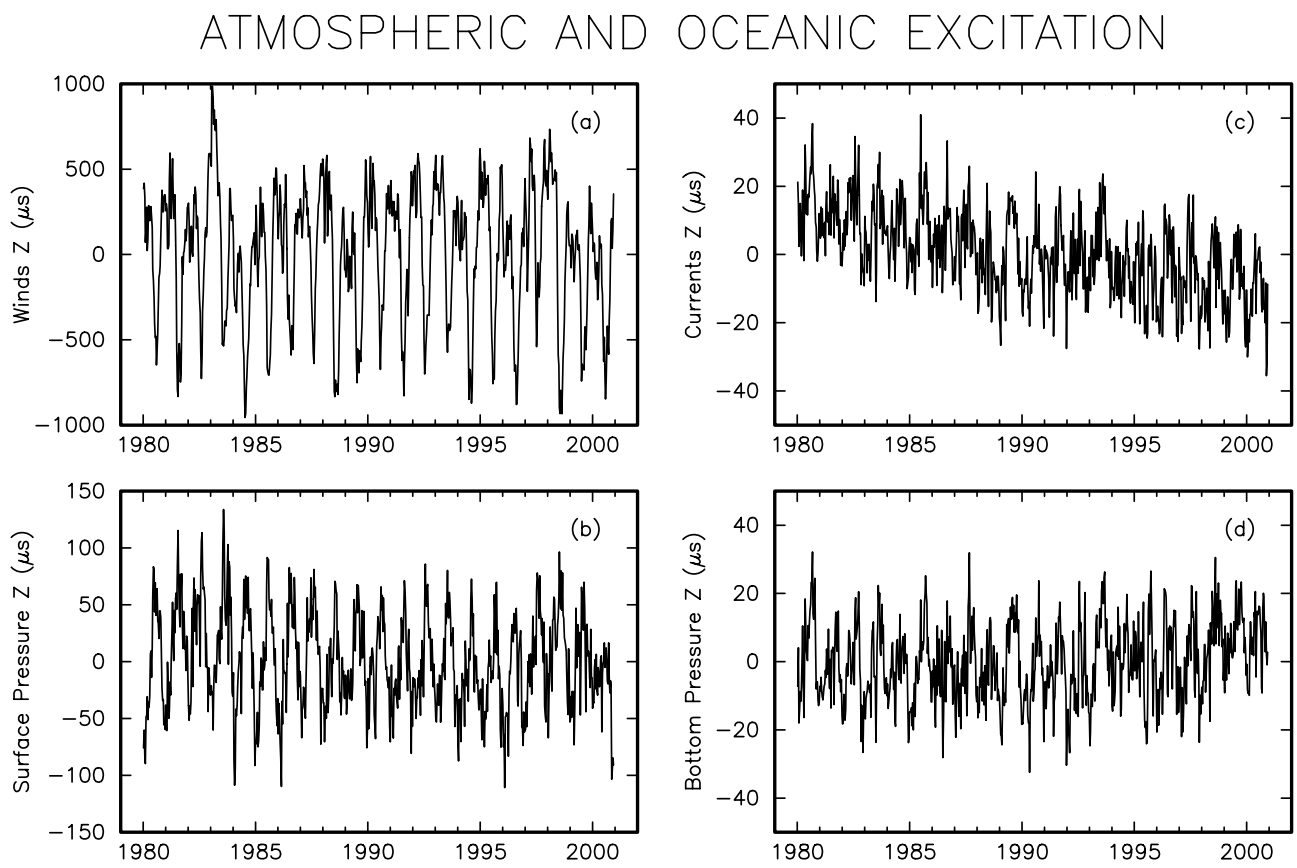

Figure 3. The *z*-component of the angular momentum, in equivalent length-of-day units, associated with (a) atmospheric winds, (b) atmospheric surface pressure variations, (c) oceanic currents, and (d) ocean-bottom pressure variations. The angular momentum associated with atmospheric surface pressure variations has been computed assuming the oceans respond as an inverted barometer to the imposed surface pressure variations. For purposes of clarity of display, 10-day averages are shown. The mean has been removed from all series.

primarily caused by annual and semiannual changes in the angular momentum of the zonal winds [*Rosen and Salstein*, 1985, 1991; *Naito and Kikuchi*, 1990, 1991; *Dickey et al.*, 1993; *Rosen*, 1993; *Höpfner*, 1998; *Aoyama and Naito*, 2000]. In this section, the relative contribution of atmospheric surface pressure and of oceanic current and bottom pressure to exciting seasonal length-of-day variations during 1980–2000 is assessed.

[21] Power spectra and coherence of the observed LOD variations and those due to zonal winds at frequencies less than 6 cycles per year (cpy) are shown in Figure 4. The spectra have been computed by the multitaper method [*Percival and Walden*, 1993] using a resolution bandwidth of $2f_R$ where $f_R \equiv 1/N\Delta t$ is the fundamental, or Rayleigh, frequency with N being the number of samples in the time series (7650), Δt being the sampling interval (1 day), and hence $N\Delta t$ being the length of the time series (21 years). A simple unweighted average of the resulting first three eigenspectra was then formed to obtain the spectra shown in Figure 4. The coherence and phase estimates were obtained by averaging over 11 frequency intervals and the 95% and 99% confidence limits of the squared magnitude of the coherence are indicated by the horizontal dashed lines in the middle panel. As can be seen, there is remarkable agreement between the observed LOD variations and those due to zonal winds at all frequencies less than 6 cpy except for the lowest frequencies near 0 cpy (a mean and trend have been removed from the series prior to computing their spectra and coherence). The discrepancy at decadal periods will be discussed in the section on the decadal LOD variations below. Here the agreement between the observed and modeled LOD variations at the annual frequency and its higher harmonics is discussed.

[22] Peaks in the power spectra of both the observed variations (black curve) and in those caused by winds (red curve) are clearly seen in the top panel of Figure 4 at the annual frequency (1 cpy) as well as at its first and second harmonics, the semiannual frequency (2 cpy), and the terannual frequency (3 cpy), respectively. Spectral peaks are not seen at higher harmonics of the annual. Since tidal variations have been removed from the LOD observations, the signals at the annual, semiannual, and terannual frequencies are not tidal in origin; rather, as shown by Figure 4 and in more detail below, they are caused primarily by changes in the atmospheric winds.

[23] In order to compare the observed and modeled LOD variations at the annual, semiannual, and terannual frequencies, mean, trend, and periodic terms at these frequencies were fit to the observed and modeled series. Since no uncertainty estimates are available for the atmospheric and

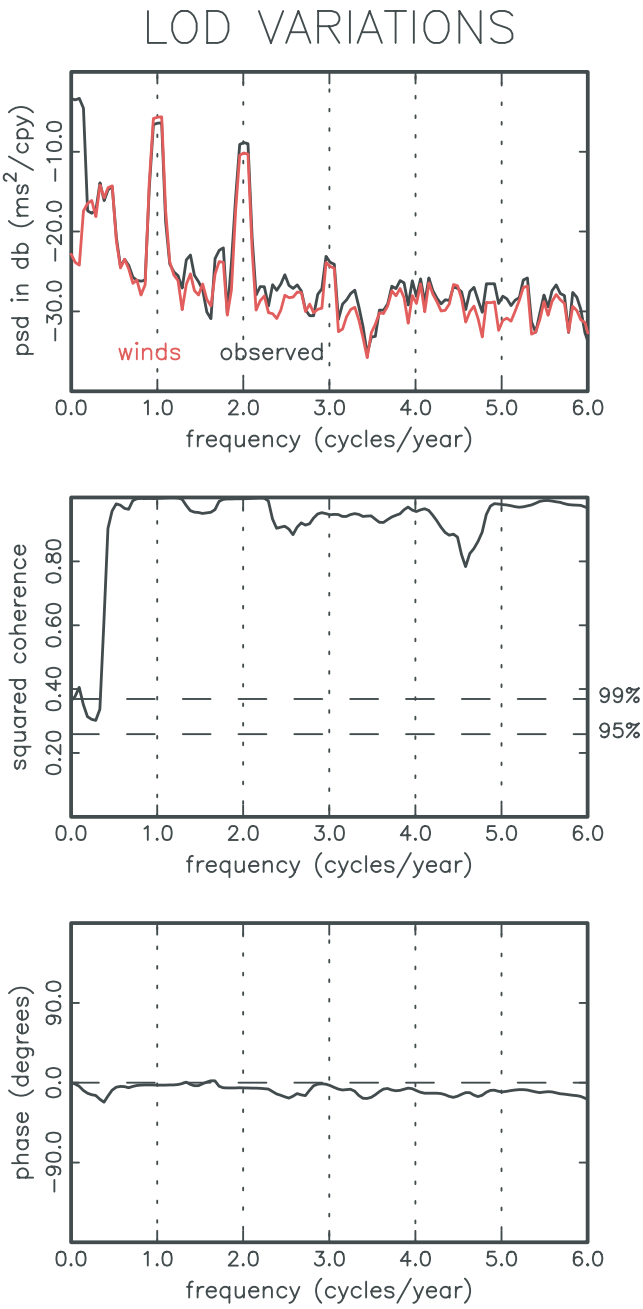

Figure 4. (top) Power spectra, (middle) squared magnitude of the coherence, and (bottom) phase of the observed length-of-day variations during 1980–2000 and those due to atmospheric winds below 10 hPa. The power spectral density (psd) estimates in the top panel, given in decibels (db), were computed by the multitaper method with the spectrum of the observed variations shown in black and that due to the winds shown in red. The horizontal dashed lines in the middle panel indicate the 95% and 99% confidence levels of the squared magnitude of the coherence between the observed and wind-driven LOD variations, with the bottom panel showing their phase spectrum.

oceanic angular momentum values, this fit was obtained using unweighted least squares. For consistency, unweighted least squares was also used to obtain the fit to the observed values even though uncertainty estimates are available for them. The uncertainties assigned to the fitted parameters and given in Tables 1 and 2 are the 1σ formal uncertainties computed using the standard deviation of the postfit residuals as an estimate of the mean uncertainty of the observed or modeled values. The uncertainties thus determined can be considered realistic in the sense that the resulting postfit residuals have a reduced chi-square of one.

[24] Table 1 shows the results of this fit for the amplitude A and phase α of the observed and modeled LOD variations at the annual, semiannual, and terannual frequencies with A and α being defined by the expression

$$\Delta\Lambda(t) = A\cos[\sigma(t - t_o) - \alpha], \tag{7}$$

where σ is the annual, semiannual, or terannual frequency and the reference date t_o is January 1, 1990. As can be seen, annual length-of-day changes are predominantly caused by annual changes in the angular momentum of the zonal winds. The angular momentum caused by mass redistribution within the atmosphere, or, equivalently, caused by surface pressure changes, is seen to have an amplitude only 12% of that observed and to be out-of-phase with the observations. The effects of oceanic currents and of mass redistribution within the oceans, or, equivalently, of ocean-bottom pressure changes, are each less than 3% of that observed and are also out-of-phase with the observed annual variations. The combined effect of oceanic currents and surface and bottom pressure variations, being out-of-phase with the effect of the winds, acts to reduce the effect of the winds so that the sum total of all atmospheric and oceanic processes at the annual frequency has an amplitude about 8% less than that observed and a phase difference of only 2 degrees (deg).

[25] The left panel of Figure 5 shows a phasor diagram of the annual component of the observed (obs) length-of-day variations during 1980–2000 and of the effects on the length-of-day of atmospheric winds (wind), surface pressure (press), and the oceans (ocn; the sum of the effects of the currents and bottom pressure). Adding oceanic effects to those of the atmosphere is seen to move the modeled variation farther away from that observed. The discrepancy that remains between the observed and modeled LOD variations is 33.4 μs in amplitude and 12.2 deg in phase. Here and in the following paragraphs on the semiannual and terannual components, the discrepancy amplitudes and phases given are those of the residual phasors formed by removing the sum total of all modeled atmospheric and oceanic effects from that observed.

[26] Semiannual LOD variations are also seen to be predominantly caused by changes in the angular momentum of the zonal winds. The effects of semiannual atmospheric surface pressure and oceanic current and bottom pressure changes on the length-of-day are each less than 3% of that observed and exhibit little agreement with the observed phase. The total effect of all atmospheric and oceanic processes at the semiannual frequency has an amplitude about 12% less than that observed and a phase difference of 4.1 deg. The middle panel of Figure 5 shows the phasor diagram of the semiannual component of the observed and modeled LOD variations. Adding oceanic effects to those of the atmosphere appears to bring the modeled variation

Table 1. Seasonal LOD Variations During 1980–2000[a]

	Annual		Semiannual		Terannual	
Excitation Process	Amplitude, μs	Phase, Degrees	Amplitude, μs	Phase, Degrees	Amplitude, μs	Phase, Degrees
Observed	373.4 ± 7.2	32.8 ± 1.1	276.7 ± 7.2	−116.8 ± 1.5	50.7 ± 7.2	37.7 ± 8.2
			Atmospheric			
Winds (ground to 10 hPa)	402.6 ± 3.4	33.9 ± 0.5	240.2 ± 3.3	−110.2 ± 0.8	46.1 ± 3.4	44.8 ± 4.2
Surface pressure (i.b.)	44.5 ± 0.5	−152.3 ± 0.7	6.3 ± 0.5	121.9 ± 4.9	4.7 ± 0.5	−108.3 ± 6.6
Winds and surface pressure	358.4 ± 3.4	34.7 ± 0.5	236.4 ± 3.4	−111.4 ± 0.8	42.0 ± 3.4	41.9 ± 4.7
			Oceanic			
Currents	7.6 ± 0.2	−156.4 ± 1.5	1.9 ± 0.2	124.2 ± 6.0	1.4 ± 0.2	57.5 ± 8.1
Bottom pressure	8.7 ± 0.2	−139.5 ± 1.2	3.9 ± 0.2	170.1 ± 2.7	0.3 ± 0.2	−42.8 ± 34.4
Currents and bottom pressure	16.1 ± 0.3	−147.4 ± 1.2	5.4 ± 0.3	155.6 ± 3.6	1.4 ± 0.3	44.7 ± 14.4
			Atmospheric and Oceanic			
Winds and currents	395.1 ± 3.4	34.1 ± 0.5	239.1 ± 3.4	−110.5 ± 0.8	47.4 ± 3.4	45.2 ± 4.1
Surface and bottom pressure	53.0 ± 0.6	−150.2 ± 0.7	9.4 ± 0.6	140.1 ± 3.7	4.8 ± 0.6	−104.9 ± 7.3
			Total			
Total of all atmos. and oceanic	342.4 ± 3.5	34.8 ± 0.6	236.2 ± 3.5	−112.7 ± 0.8	43.3 ± 3.5	42.0 ± 4.6

[a]Details: i.b., inverted barometer; atmos., atmospheric; reference date for phase is January 1, 1990.

slightly closer to that observed although a discrepancy of 44.4 μs in amplitude and −139.0 deg in phase still remains. The results obtained here for the annual and semiannual variations of the length-of-day during 1980–2000 are consistent with those obtained by *Gross* [2003a] for the shorter interval 1985–1995.

[27] As with the annual and semiannual variations, changes in the length-of-day at the terannual frequency are also predominantly caused by changes in the angular momentum of the zonal winds. The effect of atmospheric surface pressure changes is only about 9% of that observed and exhibits little agreement in phase. There is little indication of a terannual change in the angular momentum of ocean-bottom pressure variations, and the amplitude of the effect of oceanic currents is less than 3% of that observed but with a similar phase. The total effect of all atmospheric and oceanic processes at the terannual frequency has an amplitude about 15% less than that observed and a phase difference of 4.3 deg. The right panel of Figure 5 shows the phasor diagram of the terannual component of the observed and modeled LOD variations. Adding oceanic effects to those of the atmosphere is seen to bring the modeled variation slightly closer to that observed, with a remaining discrepancy of 8.1 μs in amplitude and 14.2 deg in phase.

[28] The discrepancies that remain at the annual, semiannual, and terannual frequencies after atmospheric and oceanic effects are removed from that observed may reflect errors in the observed and/or modeled LOD variations at these frequencies, but may also indicate that other processes are important in causing seasonal length-of-day changes. Since the top of the atmospheric general circulation model

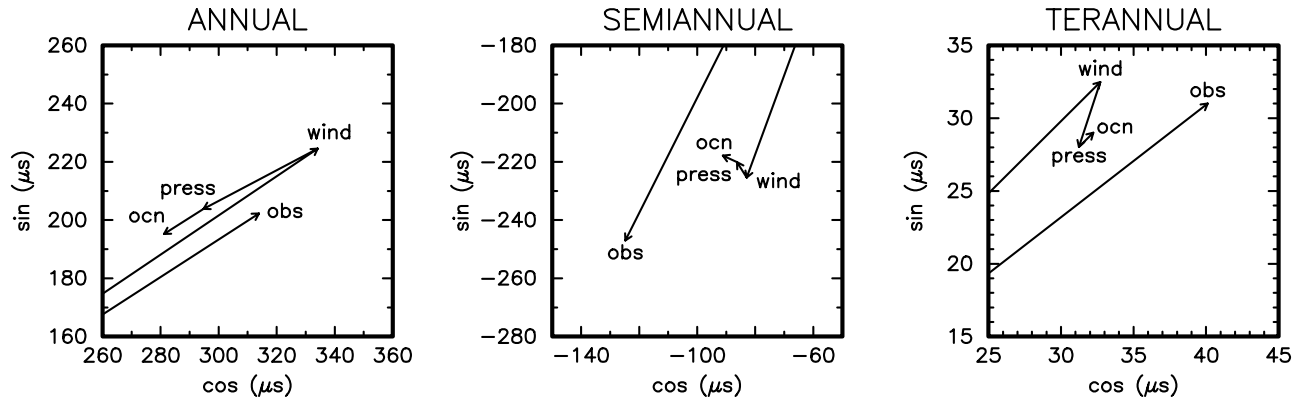

Figure 5. Phasor diagrams of the (left) annual, (middle) semiannual, and (right) terannual components of observed length-of-day variations (obs) during 1980–2000 and of the effects on LOD during this time period of atmospheric winds below 10 hPa (wind), surface pressure (press), and the oceans (ocn). The atmospheric surface pressure term was computed by assuming that the oceans respond as an inverted barometer to the imposed surface pressure variations. The oceanic results include the effects of both currents and ocean-bottom pressure. The reference date for the phase is January 1, 1990 which in the diagram is measured counterclockwise starting from a horizontal position. Note the change in scale of the terannual phasor diagram.

Table 2. Seasonal LOD Variations During 1992–2000[a]

	Annual		Semiannual		Terannual	
Excitation Process	Amplitude, μs	Phase, Degrees	Amplitude, μs	Phase, Degrees	Amplitude, μs	Phase, Degrees
Observed	369.0 ± 6.4	31.6 ± 1.0	294.3 ± 6.3	−116.5 ± 1.2	52.4 ± 6.4	20.9 ± 7.0
Atmospheric						
Winds (ground to 10 hPa)	414.8 ± 5.0	34.7 ± 0.7	244.3 ± 5.0	−110.0 ± 1.2	54.1 ± 5.0	30.4 ± 5.3
Winds (10hPa to 0.3 hPa)	20.5 ± 0.3	−161.0 ± 0.9	29.4 ± 0.3	−122.7 ± 0.6	3.5 ± 0.3	−165.7 ± 5.1
All winds (ground to 0.3 hPa)	395.1 ± 5.0	35.5 ± 0.7	273.1 ± 5.0	−111.3 ± 1.0	50.7 ± 5.0	31.4 ± 5.6
Surface pressure (i.b.)	37.4 ± 0.8	−154.6 ± 1.3	9.2 ± 0.8	113.3 ± 5.1	2.6 ± 0.8	−48.8 ± 18.1
All winds and surface pressure	358.3 ± 5.1	36.5 ± 0.8	266.7 ± 5.1	−112.7 ± 1.1	51.2 ± 5.1	28.6 ± 5.7
Oceanic						
Currents	7.6 ± 0.3	−165.5 ± 2.3	0.9 ± 0.3	115.5 ± 18.7	1.6 ± 0.3	35.9 ± 11.1
Bottom pressure	7.9 ± 0.3	−148.4 ± 2.2	3.1 ± 0.3	176.7 ± 5.5	1.0 ± 0.3	−67.3 ± 16.4
Currents and bottom pressure	15.3 ± 0.5	−156.8 ± 2.0	3.6 ± 0.5	163.4 ± 8.6	1.7 ± 0.5	−0.6 ± 18.4
Atmospheric and Oceanic						
All winds and currents	388.0 ± 5.0	35.9 ± 0.7	272.5 ± 5.0	−111.5 ± 1.1	52.3 ± 5.0	31.6 ± 5.5
Surface and bottom pressure	45.2 ± 0.9	−153.5 ± 1.2	10.9 ± 0.9	127.9 ± 4.9	3.6 ± 0.9	−54.1 ± 15.1
Total of all Atmospheric and Oceanic						
Without winds above 10 hPa	363.0 ± 5.2	36.1 ± 0.8	238.1 ± 5.2	−112.4 ± 1.3	56.1 ± 5.2	26.9 ± 5.3
With winds above 10 hPa	343.5 ± 5.2	37.1 ± 0.9	267.1 ± 5.2	−113.5 ± 1.1	52.7 ± 5.2	27.7 ± 5.7

[a]Details: i.b., inverted barometer; reference date for phase is January 1, 1990.

used by the NCEP/NCAR reanalysis project is at 10 hPa, a notable omission to the processes listed in Table 1 is the effect of the atmospheric winds above 10 hPa. Although only 1% of the atmospheric mass is located in that region of the atmosphere, the strength of the zonal winds there is great enough that they have a noticeable effect on seasonal length-of-day variations [*Rosen and Salstein*, 1985, 1991; *Dickey et al.*, 1993; *Rosen*, 1993; *Höpfner*, 2001].

5. Upper Atmospheric Winds

[29] As their contribution to the Upper Atmosphere Research Satellite (UARS), the United Kingdom Meteorological Office (UKMO) produced a set of global meteorological analyses, including the wind fields, from the ground to 0.3 hPa. This wind data set, which spans October 1991 to August 2001, is available from the British Atmospheric Data Centre and the angular momentum of the winds from 10 hPa to 0.3 hPa has been computed using this data set. Table 2 shows the effect of these upper atmosphere winds on seasonal length-of-day variations during 1992–2000. As can be seen, the angular momentum of the zonal winds above 10 hPa at the annual, semiannual, and terannual frequencies is much greater than the angular momentum of either oceanic currents or bottom pressure.

[30] At the annual frequency, the angular momentum of the zonal winds above 10 hPa is nearly out-of-phase with that below 10 hPa but in-phase with the angular momentum of surface pressure and oceanic current and bottom pressure changes. Without the winds above 10 hPa, the total effect of all atmospheric and oceanic processes at the annual frequency has an amplitude differing from that observed by less than 2% and a phase difference of 4.5 deg. But when the effect of the winds above 10 hPa is included with the other processes, the total amplitude is reduced so that it is 7% less than that observed with a phase difference of 5.5 deg.

[31] The left panel of Figure 6 shows a phasor diagram of the annual component of the observed (obs) length-of-day variations during 1992–2000 and of the effects on the length-of-day of atmospheric winds below 10 hPa (wind), winds above 10 hPa (upper), surface pressure (press), and the oceans (ocn; the sum of the effects of the currents and bottom pressure). As during 1980–2000, adding oceanic effects to those of the atmosphere is seen to move the modeled variation farther away from that observed. The discrepancy that remains between the observed and modeled LOD variations is 45.2 μs in amplitude and 2.7 deg in phase.

[32] At the semiannual frequency, the angular momentum of the zonal winds above 10 hPa is nearly in-phase with that below 10 hPa. In this case, adding the effect of the winds above 10 hPa acts to bring the total effect of all atmospheric and oceanic processes closer to that observed. Without the winds above 10 hPa, the total effect of all atmospheric and oceanic processes at the semiannual frequency has an amplitude 19% less than that observed and a phase difference of 4.1 deg. But when the effect of the winds above 10 hPa is included with the other processes, their total amplitude is increased so that it is 9% less than that observed with a phase difference of 3.0 deg. The middle panel of Figure 6 shows the phasor diagram of the semiannual component of the observed and modeled LOD variations. Adding oceanic effects to those of the atmosphere is seen to bring the modeled variation somewhat closer to that observed although a discrepancy of 17.1 μs in amplitude and −179.2 deg in phase still remains.

[33] At the terannual frequency, the angular momentum of the zonal winds above 10 hPa is, like at the annual frequency, nearly out-of-phase with that below 10 hPa. However, unlike the annual frequency, adding the effect of the winds above 10 hPa acts to bring the total effect of all atmospheric and oceanic processes closer to that observed. Without the winds above 10 hPa, the total effect

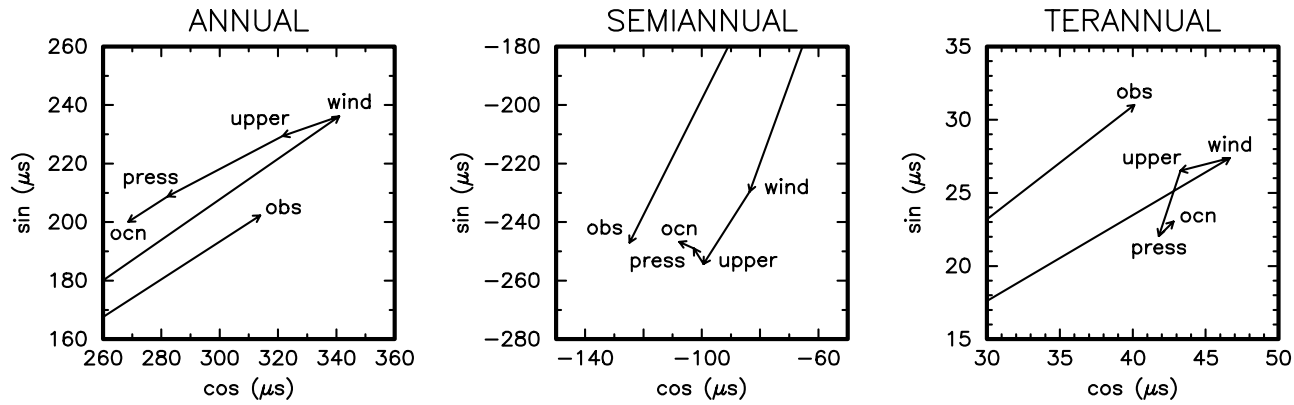

Figure 6. Phasor diagrams of the (left) annual, (middle) semiannual, and (right) terannual components of the observed length-of-day variations (obs) during 1992–2000 and of the effects on the LOD during this time period of atmospheric winds below 10 hPa (wind), winds above 10 hPa (upper), surface pressure (press), and the oceans (ocn). The atmospheric surface pressure term was computed by assuming that the oceans respond as an inverted barometer to the imposed surface pressure variations. The oceanic results include the effects of both currents and ocean-bottom pressure. The reference date for the phase is January 1, 1990 which in the diagram is measured counterclockwise starting from a horizontal position. Note the change in scale of the terannual phasor diagram.

of all atmospheric and oceanic processes at the terannual frequency has an amplitude 7% greater than that observed and a phase difference of 6.0 deg. However, when the effect of the winds above 10 hPa is included with the other processes, their total amplitude is reduced so that it is nearly the same as that observed with a phase difference of 6.8 deg. The right panel of Figure 6 shows the phasor diagram of the terannual component of the observed and modeled LOD variations. Adding oceanic effects to those of the atmosphere appears to bring the modeled variation slightly closer to that observed, with a remaining discrepancy of 8.4 μs in amplitude and 108.6 deg in phase.

[34] The angular momentum of the upper atmospheric zonal winds between 10 hPa and 0.3 hPa clearly has a noticeable effect on seasonal length-of-day variations. In fact, their effect is much larger than that of either oceanic currents or bottom pressure changes. At the annual frequency, the amplitude of the angular momentum of the upper atmospheric zonal winds is 2.5 times larger than the effect of either oceanic currents or bottom pressure changes; at the semiannual frequency it is nearly 10 times larger than the effect of bottom pressure changes and more than 30 times larger than the effect of oceanic currents; and at the terannual frequency it is 3.5 times as large as the effect of ocean bottom pressure changes and twice as large as the effect of oceanic currents.

[35] There are still discrepancies between the observed and modeled seasonal variations even after including the effect of the zonal winds above 10 hPa. Effects associated with hydrologic processes may be important at these frequencies, but they are difficult to accurately estimate given the state of the current generation global hydrologic models [*Chen et al.*, 2000b].

6. Intraseasonal Variations

[36] Estimates of the coherence at high frequencies (not shown) between the observed LOD variations and those caused by the sum of atmospheric wind and surface pressure and oceanic current and bottom pressure variations indicate a loss of coherence at periods shorter than about 4 days. A 4-day running mean was therefore applied to the observed and modeled data sets used here in order to eliminate signals having periods less than 4 days. Before this was done, seasonal signals were first removed from the data sets by least squares fitting and removing a mean, a trend, and periodic terms at the annual, semiannual, and terannual frequencies. A highpass filter with a cutoff frequency of 1 cpy was then applied to the data sets in order to isolate the intraseasonal frequency band. Thus the intraseasonal frequency band considered here consists of signals having periods between 4 days and 1 year excluding signals at the annual, semiannual, and terannual frequencies.

[37] Figure 7 shows the observed and modeled LOD variations on intraseasonal timescales during 1997. As can be seen, there is remarkable agreement between the observed variations (black curve) and that due to atmospheric winds (red curve). Adding the effects of surface pressure and oceanic currents and bottom pressure to that of the winds (blue curve) is seen to lead to even better agreement with the observations. Results for other intervals during 1980–2000 are similar to that shown in Figure 7 for 1997.

[38] Table 3 gives the percentage of the observed LOD variance explained by the modeled processes along with the correlation between the observed and modeled series in the intraseasonal frequency band during 1980–2000. The sample autocorrelation functions (ACFs, not shown) of the observed and modeled series indicate an effective decorrelation length (given by the e-folding time of the central peak of the ACF) for these series of about 12 days. Since each series spans 7650 days, an effective decorrelation length of about 12 days implies that these series have about 7650/12, or 637, effective degrees of freedom. Hence the 99% significance level for the correlations in the intraseasonal frequency band is estimated to be about 0.10 after account-

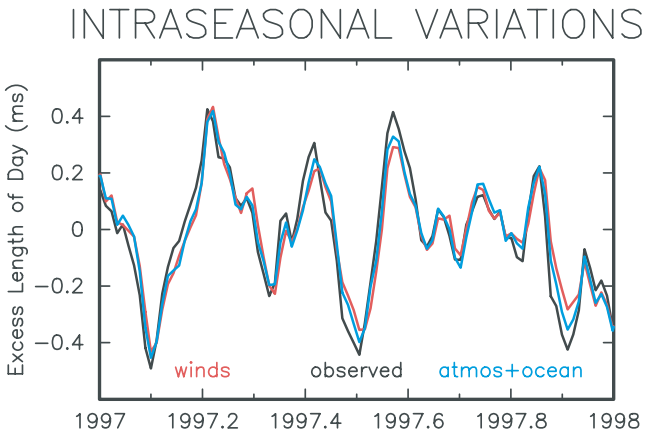

Figure 7. Observed length-of-day variations (black); variations caused by the modeled atmospheric winds (red); and variations caused by the sum of the modeled atmospheric winds, surface pressure, oceanic currents, and bottom pressure (blue) on intraseasonal timescales during 1997. Intraseasonal variations considered here have periods ranging between 4 days and 1 year, excluding signals at the annual, semiannual, and terannual frequencies. The atmospheric surface pressure term is that computed assuming the oceans respond as an inverted barometer to the imposed surface pressure variations. The contribution to intraseasonal LOD variations of the winds between 10 hPa and 0.3 hPa is included in the red and blue curves. The mean has been removed from all series.

ing for the reduction in the degrees of freedom in this manner.

[39] As with the seasonal variations, atmospheric winds are seen to be the dominant mechanism exciting intraseasonal length-of-day variations during 1980–2000. The effects of atmospheric winds explain 83.6% of the observed intraseasonal variance and have a correlation coefficient of 0.92 with the observations. Atmospheric surface pressure, oceanic currents, and bottom pressure are seen to have only a minor effect on intraseasonal length-of-day changes, each explaining only about 2–4% of the observed variance. However, including the effect of surface pressure changes with that of the winds increases the variance explained from 83.6% to 87.5% and increases the correlation coefficient with the observations from 0.92 to 0.94. Additionally including the effects of changes in oceanic currents and bottom pressure further increases the variance explained from 87.5% to 89.1% and further increases the correlation coefficient from 0.94 to 0.95. Thus, closer agreement with the observations in the intraseasonal frequency band is obtained when the effects of oceanic processes are added to that of atmospheric.

[40] In the previous section, the upper atmospheric winds from 10 hPa to 0.3 hPa were found to have a larger effect than either oceanic currents or bottom pressure on seasonal length-of-day variations. Table 4 shows the effect of these upper atmospheric winds on length-of-day variations in the intraseasonal frequency band during 1992–2000. As can be seen, they account for only 1.1% of the observed intraseasonal LOD variance during this time period. Oceanic currents and surface and bottom pressure variations are each about 3 times more effective than are the upper atmospheric winds in causing the length-of-day to change on intraseasonal timescales.

Table 3. Intraseasonal LOD Variations During 1980–2000[a]

Excitation Process	Variance Explained, %	Correlation
Atmospheric		
Winds (ground to 10 hPa)	83.6	0.95
Surface pressure (i.b.)	4.2	0.21
Winds and surface pressure (i.b.)	87.5	0.94
Oceanic		
Currents	3.4	0.32
Bottom pressure	2.2	0.22
Currents and bottom pressure	5.2	0.30
Atmospheric and Oceanic		
Winds and currents	85.0	0.92
Surface (i.b.) and bottom pressure	5.9	0.25
Total		
Total of all atmospheric and oceanic	89.1	0.95

[a]Details: %, percentage; i.b., inverted barometer; 99% significance level for correlations is 0.10; intraseasonal variations considered here have periods ranging between 4 days and 1 year excluding signals at the annual, semiannual, and terannual frequencies.

[41] Table 4 also shows that the total of all atmospheric and oceanic processes, including the effect of the upper atmospheric winds from 10 hPa to 0.3 hPa, explains 92.2% of the observed intraseasonal length-of-day variance during 1992–2000, and has a correlation coefficient with the observations of 0.96. Without the effect of the upper atmospheric winds, the total of all atmospheric and oceanic processes explains 91.9% of the observed variance during 1992–2000, whereas it explains 89.1% of the observed variance during 1980–2000 (see Table 3). This increase by 2.8% in the amount of the observed variance explained may

Table 4. Intraseasonal LOD Variations During 1992–2000[a]

Excitation Process	Variance Explained, %	Correlation
Atmospheric		
Winds (ground to 10 hPa)	85.8	0.93
Winds (10 hPa to 0.3 hPa)	1.1	0.12
All winds (ground to 0.3 hPa)	85.9	0.93
Surface pressure (i.b.)	3.3	0.18
All winds and surface pressure (i.b.)	90.2	0.95
Oceanic		
Currents	4.1	0.36
Bottom pressure	3.3	0.30
Currents and bottom pressure	7.0	0.36
Atmospheric and Oceanic		
All winds and currents	87.4	0.94
Surface (i.b.) and bottom pressure	5.9	0.25
Total of all Atmospheric and Oceanic		
Without winds above 10 hPa	91.9	0.96
With winds above 10 hPa	92.2	0.96

[a]Details: %, percentage; i.b., inverted barometer; 99% significance level for correlations is 0.18; intraseasonal variations considered here have periods ranging between 4 days and 1 year excluding signals at the annual, semiannual, and terannual frequencies.

be a reflection of the improving accuracies of the observed and/or modeled data sets during this time period.

7. Decadal Variations

[42] Length-of-day variations on decadal timescales are thought to be caused primarily by interactions between the mantle and core [e.g., *Ponsar et al.*, 2003, and references therein]. The ineffectiveness of atmospheric winds in exciting LOD variations at low frequencies can be seen by examining Figure 4. Remarkable agreement between the observed LOD variations and that caused by atmospheric winds is shown in Figure 4 at all but the very lowest frequencies. At frequencies less than about 1/5 cpy the observed power increases whereas that of the atmospheric winds decreases and the squared magnitude of the coherence between the observed variations and those caused by the winds drops below the 99% significance level.

[43] Atmospheric surface pressure and oceanic currents and bottom pressure are also ineffective in exciting length-of-day variations at frequencies less than about 1/5 cpy. In the top panel of Figure 8 the power spectrum of the difference between the observed LOD variations and those caused by atmospheric winds (black curve) is compared with the power spectrum of the variations caused by surface pressure changes (red curve) and with the power spectrum of the sum of the variations caused by surface pressure, oceanic currents, and ocean-bottom pressure (blue curve). As can be seen, the power spectra of both the surface pressure variations and of the sum of the surface pressure, oceanic currents, and bottom pressure variations remain relatively flat at frequencies lower than the annual harmonic. Therefore these processes cannot explain the increased power at frequencies less than about 1/5 cpy evident in the spectrum of the difference between the observed LOD variations and those caused by atmospheric winds.

8. Interannual Variations

[44] Figure 9 shows the observed and modeled length-of-day variations on interannual timescales obtained by applying a bandpass filter with cutoff frequencies of 1/5 cpy and 1 cpy to the data sets. As above, seasonal signals were first removed from the data sets by least squares fitting and removing a mean, a trend, and periodic terms at the annual, semiannual, and terannual frequencies. Except during 2000, there is remarkable agreement between the observed length-of-day variations (black curve) and that caused by the atmospheric winds (red curve). Including the effects of surface pressure, oceanic currents, and ocean-bottom pressure with that of the winds (blue curve) changes this agreement only marginally.

[45] Table 5 gives the percentage of the observed interannual length-of-day variance explained by the modeled processes along with the correlation between the observed and modeled data sets. The 99% significance level for the correlations is estimated to be 0.38 after accounting for the reduction in the degrees of freedom that was determined from the width of the central peak of the autocorrelation functions.

[46] As can be seen from Table 5, atmospheric winds are the dominant mechanism causing the length-of-day to change on interannual timescales during 1980–2000, explaining 85.8% of the observed variance, and having a correlation coefficient of 0.93 with the observations. The effect of atmospheric surface pressure changes explains only 2.6% of the observed variance and is not significantly correlated at the 99% significance level with the observations. However, including the effect of surface pressure changes with that of the winds increases the observed variance explained from 85.8% to 87.3%.

[47] Oceanic currents and bottom pressure changes are seen to have only a marginal effect on interannual length-of-day variations, each explaining less than 1% of the observed variance, and neither being significantly correlated with the observations. However, including their effects with those of the atmospheric winds and surface pressure changes increases the observed variance explained from 87.3% to 87.9%, and increases the correlation coefficient with the observations from 0.93 to 0.94. Although this improvement in the observed variance explained and correlation is marginal, it positively demonstrates that better agreement with the observations in the interannual frequency band during 1980-2000 is obtained when the effect of oceanic processes are included with those of the atmosphere.

9. Correlation With SOI

[48] The El Niño/Southern Oscillation (ENSO) phenomenon is a global-scale oscillation of the coupled atmosphere-ocean system characterized by fluctuations in ocean temperatures and atmospheric surface pressure in the tropical Pacific [e.g., *Philander*, 1990]. During the warm phase of ENSO the sea surface temperature in the eastern tropical Pacific is warmer than usual, the surface pressure over Indonesia and the western tropical Pacific is higher than usual, and the surface pressure over the eastern tropical Pacific is lower than usual. During the cool phase of ENSO the conditions are reversed with the sea surface temperature in the eastern tropical Pacific being cooler than usual, the surface pressure over Indonesia and the western tropical Pacific being lower than usual, and the surface pressure over the eastern tropical Pacific being higher than usual.

[49] A number of indices have been developed to quantify the strength of the ENSO phenomenon, including the Southern Oscillation Index (SOI). The SOI is the normalized difference between the Tahiti and Darwin, Australia, standardized surface pressure values and as such is a measure of the changes in surface pressure that occur between the eastern and western tropical Pacific during ENSO. However, the SOI is highly correlated with other ENSO indices such as those based upon the sea surface temperature in the tropical Pacific, especially within the "Niño 3" region of 5°N to 5°S latitude and 150°W to 90°W longitude. In this study the SOI will be used as an index of the strength of the ENSO phenomenon, encompassing both its atmospheric and oceanic components.

[50] Many studies have shown that observed LOD variations on interannual timescales, as well as interannual variations in the angular momentum of the zonal winds, are negatively correlated with the SOI, reflecting the impact on the length-of-day of changes in the zonal winds associated with ENSO events (for reviews see *Eubanks* [1993] and *Rosen* [1993]). Here the possibility that interannual

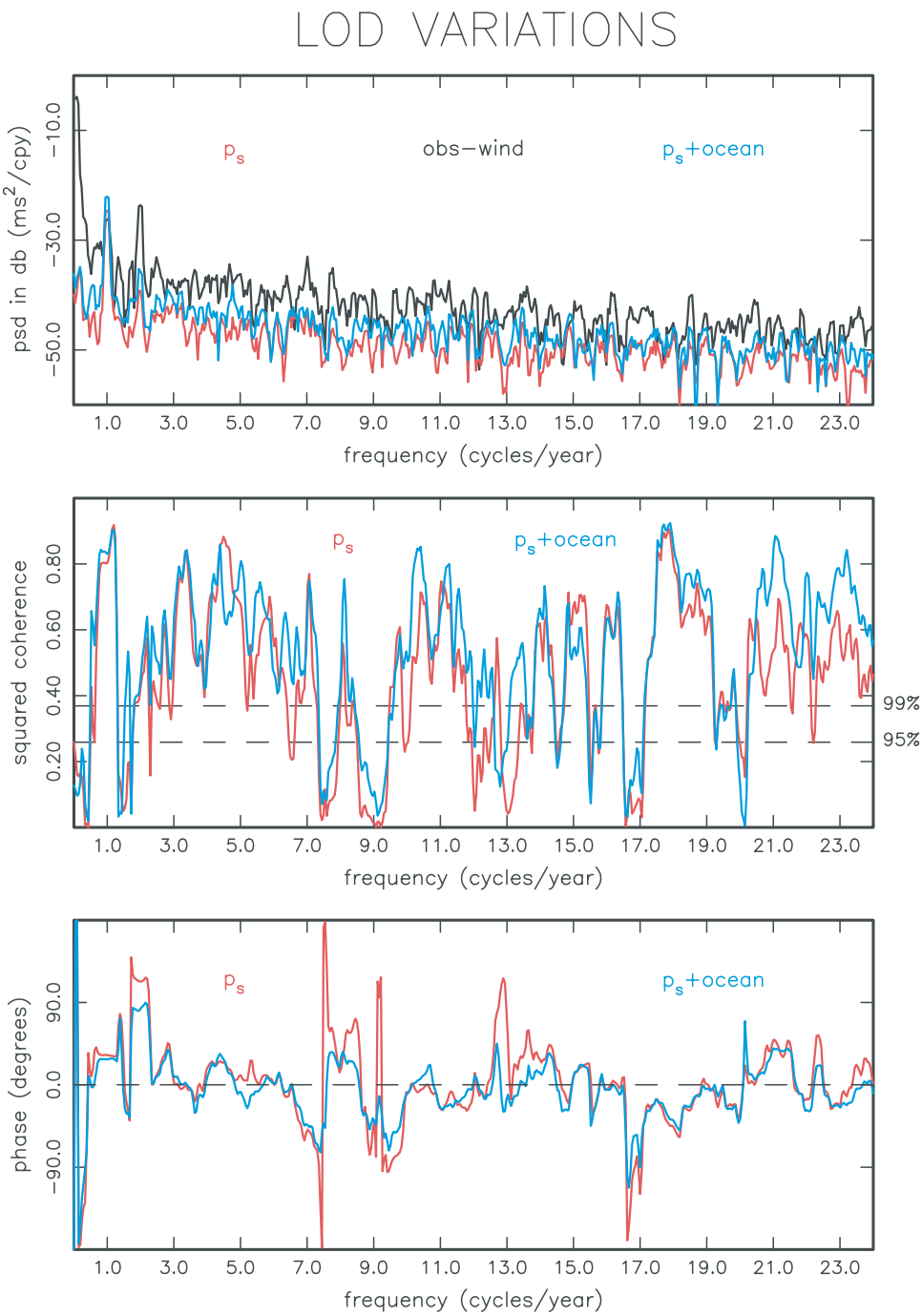

Figure 8. (top) Power spectral density (psd) estimates in decibels (db) of the observed LOD variations during 1980–2000 from which the effects of winds have been removed (black curve), of the variations due to atmospheric surface pressure p_s changes (red curve), and of the variations due to the sum of surface pressure, oceanic currents, and ocean-bottom pressure changes (blue curve). (middle) The squared magnitude of the coherence and (bottom) the phase between the observed LOD variations from which the effects of the winds have been removed and either the variations due to surface pressure changes (red curves) or the variations due to the sum of surface pressure, oceanic currents, and ocean-bottom pressure changes (blue curves). Variations at the annual, semiannual, and terannual frequencies were not removed from the data sets prior to spectral and coherence estimation.

changes in the axial component of the oceanic angular momentum are correlated with the SOI is explored.

[51] The particular SOI series used here was obtained from NOAA's Climate Prediction Center. In order to match the spectral content of the observed and modeled interannual LOD series, a bandpass filter with cutoff frequencies of 1/5 cpy and 1 cpy was applied to the SOI series. As can be seen from Table 6, and in agreement with previous studies,

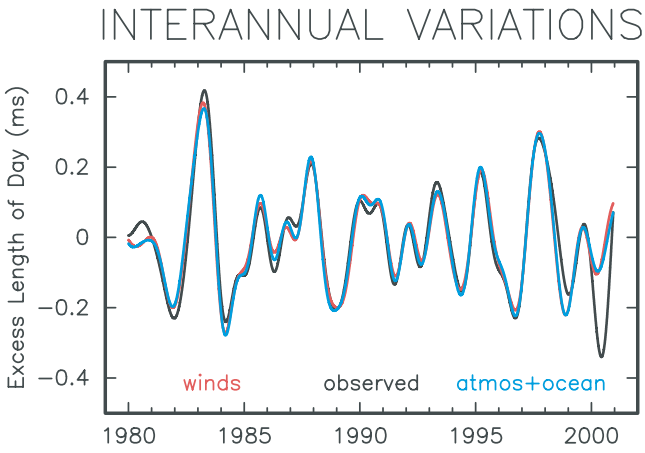

Figure 9. Observed length-of-day variations (black); variations caused by the modeled atmospheric winds (red); and variations caused by the sum of the modeled atmospheric winds, surface pressure, oceanic currents, and ocean-bottom pressure (blue) on interannual timescales during 1980–2000. The interannual frequency band ranges from 1/5 cpy to 1 cpy. The atmospheric surface pressure term is that computed assuming the oceans respond as an inverted barometer to the imposed surface pressure variations. The mean has been removed from all series.

with a correlation coefficient of −0.645 the observed LOD variations on interannual timescales are significantly negatively correlated with the SOI during 1980–2000. In fact, with a correlation coefficient of −0.719, even greater negative correlation is obtained between the SOI and interannual changes in the angular momentum of the zonal winds. Interannual variations in LOD due to changes in either atmospheric surface pressure, oceanic currents, or ocean-bottom pressure are not significantly correlated with the SOI. In fact, successively adding these effects to that of the winds decreases the correlation with the SOI, from −0.719 when just the effect of the winds are considered, to −0.713 for the sum of the effects of the winds and surface pressure, to −0.707 for the sum of the effects of the winds, currents, surface, and bottom pressure. Thus there is no evidence that oceanic angular momentum, either that due to currents or that due to changes in bottom pressure, is significantly correlated with the SOI.

10. Discussion and Summary

[52] Atmospheric and oceanic excitation of length-of-day variations during 1980–2000 has been studied here using (1) the angular momentum of surface pressure changes and zonal winds in the atmosphere below 10 hPa estimated by the NCEP/NCAR reanalysis project, (2) the angular momentum of zonal winds in the atmosphere above 10 hPa estimated by the UKMO, and (3) the angular momentum of oceanic current and bottom pressure changes estimated from the ECCO consortium's simulation of the general circulation of the oceans. As expected, the angular momentum of the zonal winds below 10 hPa was found to be the dominant mechanism causing the length-of-day to change on intraseasonal, seasonal, and interannual timescales during 1980–2000. The winds above 10 hPa were found to be more effective than the sum of oceanic current and bottom pressure changes in causing the length-of-day to change on seasonal timescales, and, except at the annual frequency, were found to be even more effective than surface pressure changes. On intraseasonal timescales, atmospheric surface pressure, oceanic currents, and ocean-bottom pressure were found to be about equally effective in causing the length-of-day to change, while the winds above 10 hPa were found to be less effective than these mechanisms. On interannual timescales, oceanic currents and ocean-bottom pressure changes were found to be only marginally effective in causing the length-of-day to change, while the available upper atmospheric wind data set, which spans October 1991 to August 2001, is too short to study its effect on interannual length-of-day variations.

[53] On intraseasonal to interannual timescales, and except at the annual frequency, closer agreement with the

Table 5. Interannual LOD Variations During 1980–2000[a]

Excitation Process	Variance Explained, %	Correlation
Atmospheric		
Winds (ground to 10 hPa)	85.8	0.93
Surface pressure (i.b.)	2.6	0.24
Winds and surface pressure (i.b.)	87.3	0.93
Oceanic		
Currents	0.6	0.14
Bottom pressure	0.4	0.09
Currents and bottom pressure	0.8	0.12
Atmospheric and Oceanic		
Winds and currents	86.2	0.93
Surface (i.b.) and bottom pressure	2.9	0.23
Total		
Total of all atmospheric and oceanic	87.9	0.94

[a]Details: %, percentage; i.b., inverted barometer; 99% significance level for correlations is 0.38; interannual frequency band ranges from 1/5 cpy to 1 cpy.

Table 6. Correlation of Interannual LOD Variations With SOI[a]

Excitation Process	Correlation Coefficient
Observed	−0.645
Atmospheric	
Winds (ground to 10 hPa)	−0.719
Surface pressure (i.b.)	−0.007
Winds and surface pressure (i.b.)	−0.713
Oceanic	
Currents	0.040
Bottom pressure	0.137
Currents and bottom pressure	0.093
Atmospheric and Oceanic	
Winds and currents	−0.717
Surface (i.b.) and bottom pressure	0.039
Total	
Total of all atmospheric and oceanic	−0.707

[a]Details: SOI, Southern Oscillation Index; i.b., inverted barometer; 99% significance level for correlations is 0.38; interannual frequency band ranges from 1/5 cpy to 1 cpy.

observations was obtained by adding the effects of oceanic currents and bottom pressure changes to those of atmospheric winds and surface pressure changes (see Tables 1–5). This is also illustrated in the top panel of Figure 8 where at nearly all but the annual frequency, it is seen that adding the effects of currents and bottom pressure changes to that of surface pressure changes brings the modeled power closer to the power of the difference between the observed LOD variations and that caused by winds during 1980–2000. This closer agreement across a broad range of frequencies when the effect of the oceans is added to that of the atmosphere was also found by *Marcus et al.* [1998] during the much shorter time interval of 1992–1994, and by *Ponte and Stammer* [2000] during 1985–1996.

[54] The discrepancies that remain between the observed and modeled length-of-day data sets could be due to either errors in the data sets and models used here, or to the action of other processes that have not been considered here such as hydrologic effects. Errors in the data sets are one possible limiting factor in closing the LOD budget during 1980–2000. This is suggested from the improved agreement between the observed and modeled LOD series in the intraseasonal frequency band that is obtained when just the results during the more recent time interval of 1992–2000 is considered. Also, *Ponte et al.* [2001] have shown that better agreement with the observations is obtained when using oceanic angular momentum series that have been estimated from an ocean model that has assimilated oceanographic data.

[55] Redistribution of mass within the atmosphere, oceans, hydrosphere, and cryosphere not only cause the Earth's rotation to change but also cause the Earth's gravitational field to change. One of the goals of the CHAMP and GRACE satellite missions is to measure temporal changes in the Earth's gravitational field. Since changes in the second-degree zonal gravitational field coefficient are related to changes in the length-of-day [e.g., *Lambeck*, 1980; *Chao and O'Connor*, 1988; *Chen et al.*, 2000a; *Gross*, 2001b, 2003b], CHAMP and GRACE will, in effect, be directly measuring variations in the length-of-day caused by mass redistribution. The availability of direct measurements of length-of-day variations caused by mass redistribution over land and, separately, within the oceans can be expected to lead to greater understanding of the mechanisms causing the length-of-day to change.

[56] **Acknowledgments.** We thank S. Dickman for his thorough review and an anonymous reviewer for additional comments, both of which led to substantial improvements to the paper. The work of R. S. G., I. F., and D. M. described in this paper was performed at the Jet Propulsion Laboratory, California Institute of Technology, under contract with the National Aeronautics and Space Administration. Support for this work was provided by the Oceanography Program of NASA's Office of Earth Science. The supercomputer used in this investigation was provided by funding from JPL Institutional Computing and Information Services and the NASA Offices of Earth Science, Aeronautics, and Space Science. This is a contribution of the Consortium for Estimating the Circulation and Climate of the Ocean (ECCO) funded by the National Oceanographic Partnership Program.

References

Aoyama, Y., and I. Naito (2000), Wind contributions to the Earth's angular momentum budgets in seasonal variation, *J. Geophys. Res.*, *105*, 12,417–12,431.

Barnes, R. T. H., R. Hide, A. A. White, and C. A. Wilson (1983), Atmospheric angular momentum fluctuations, length-of-day changes and polar motion, *Proc. R. Soc. London, Ser. A*, *387*, 31–73.

Brosche, P., and J. Sündermann (1985), The Antarctic Circumpolar Current and its influence on the Earth's rotation, *Dtsch. Hydrogr. Z.*, *38*, 1–6.

Brosche, P., J. Wünsch, A. Frische, J. Sündermann, E. Maier-Reimer, and U. Mikolajewicz (1990), The seasonal variation of the angular momentum of the oceans, *Naturwissenschaften*, *77*, 185–186.

Brosche, P., J. Wünsch, E. Maier-Reimer, J. Segschneider, and J. Sündermann (1997), The axial angular momentum of the general circulation of the oceans, *Astron. Nachr.*, *318*, 193–199.

Bryan, F. O. (1997), The axial angular momentum balance of a global ocean general circulation model, *Dyn. Atmos. Oceans*, *25*, 191–216.

Chao, B. F., and W. P. O'Connor (1988), Effect of a uniform sea-level change on the Earth's rotation and gravitational field, *Geophys. J. R. Astron. Soc.*, *93*, 191–193.

Chen, J. L., C. R. Wilson, R. J. Eanes, and B. D. Tapley (2000a), A new assessment of long-wavelength gravitational variations, *J. Geophys. Res.*, *105*, 16,271–16,277.

Chen, J. L., C. R. Wilson, B. F. Chao, C. K. Shum, and B. D. Tapley (2000b), Hydrological and oceanic excitations to polar motion and length-of-day variation, *Geophys. J. Int.*, *141*, 149–156.

Dickey, J. O., S. L. Marcus, C. M. Johns, R. Hide, and S. R. Thompson (1993), The oceanic contribution to the Earth's seasonal angular momentum budget, *Geophys. Res. Lett.*, *20*, 2953–2956.

Dukowicz, J. (1997), Steric sea level in the Los Alamos POP code—Non-Boussinesq effects, in *Numerical Methods in Atmospheric and Oceanic Modelling: The Andre Robert Memorial Volume*, edited by C. A. Lin, R. Laprise, and H. Ritchie, pp. 533–546, Can. Meteorol. Oceanogr. Soc., Ottowa, Ont., Canada.

Eubanks, T. M. (1993), Variations in the orientation of the Earth, in *Contributions of Space Geodesy to Geodynamics: Earth Dynamics*, *Geodyn. Ser.*, vol. 24, edited by D. E. Smith and D. L. Turcotte, pp. 1–54, AGU, Washington, D. C.

Frankignoul, C., and P. Müller (1979), Quasi-geostrophic response of an infinite β-plane ocean to stochastic forcing by the atmosphere, *J. Phys. Oceanogr.*, *9*, 104–127.

Frische, A., and J. Sündermann (1990), The seasonal angular momentum of the thermohaline ocean circulation, in *Earth's Rotation From Eons to Days*, edited by P. Brosche and J. Sündermann, pp. 108–126, Springer-Verlag, New York.

Greatbatch, R. J. (1994), A note on the representation of steric sea level in models that conserve volume rather than mass, *J. Geophys. Res.*, *99*, 12,767–12,771.

Greatbatch, R. J., Y. Lu, and Y. Cai (2001), Relaxing the Boussinesq approximation in ocean circulation models, *J. Atmos. Oceanic Technol.*, *18*, 1911–1923.

Gross, R. S. (2001a), Combinations of Earth orientation measurements: SPACE2000, COMB2000, and POLE2000, *JPL Publ., 01-2*, 25 pp.

Gross, R. S. (2001b), Gravity, oceanic angular momentum, and the Earth's rotation, in *Gravity, Geoid, and Geodynamics 2000*, *IAG Symp. Ser.*, vol. 123, edited by M. G. Sideris, pp. 153–158, Springer-Verlag, New York.

Gross, R. S. (2003a), Angular momentum in the Earth system, in *Proceedings of the V Hotine-Marussi Symposium on Mathematical Geodesy*, edited by F. Sanso, Springer-Verlag, New York, in press.

Gross, R. S. (2003b), CHAMP, mass displacements, and the Earth's rotation, in *First CHAMP Mission Results for Gravity, Magnetic and Atmospheric Studies*, edited by C. Reigber, H. Lühr, and P. Schwintzer, pp. 174–179, Springer-Verlag, New York.

Gross, R. S., T. M. Eubanks, J. A. Steppe, A. P. Freedman, J. O. Dickey, and T. F. Runge (1998), A Kalman filter-based approach to combining independent Earth orientation series, *J. Geod.*, *72*, 215–235.

Gross, R. S., I. Fukumori, and D. Menemenlis (2003), Atmospheric and oceanic excitation of the Earth's wobbles during 1980–2000, *J. Geophys. Res.*, *108*(B8), 2370, doi:10.1029/2002JB002143.

Höpfner, J. (1998), Seasonal variations in length of day and atmospheric angular momentum, *Geophys. J. Int.*, *135*, 407–437.

Höpfner, J. (2001), Atmospheric, oceanic, and hydrological contributions to seasonal variations in length of day, *J. Geod.*, *75*, 137–150.

Huang, R. X., and X. Jin (2002), Sea surface elevation and bottom pressure anomalies due to thermohaline forcing. Part I: Isolated perturbations, *J. Phys. Oceanogr.*, *32*, 2131–2150.

Johnson, T. J., C. R. Wilson, and B. F. Chao (1999), Oceanic angular momentum variability estimated from the Parallel Ocean Climate Model, 1988–1998, *J. Geophys. Res.*, *104*, 25,183–25,195.

Kalnay, E., et al. (1996), The NCEP/NCAR 40-year reanalysis project, *Bull. Am. Meteorol. Soc.*, *77*, 437–471.

Kantha, L. H., J. S. Stewart, and S. D. Desai (1998), Long-period lunar fortnightly and monthly ocean tides, *J. Geophys. Res.*, *103*, 12,639–12,647.

Lambeck, K. (1980), *The Earth's Variable Rotation: Geophysical Causes and Consequences*, 449 pp., Cambridge Univ. Press, New York.

Lambeck, K. (1988), *Geophysical Geodesy: The Slow Deformations of the Earth*, 718 pp., Oxford Univ. Press, New York.
Levitus, S., and T. Boyer (1994), *World Ocean Atlas 1994*, vol. 4, *Temperature*, *NOAA Atlas NESDIS 4*, 117 pp., Natl. Oceanic and Atmos. Admin., Silver Spring, Md.
Levitus, S., R. Burgett, and T. Boyer (1994), *World Ocean Atlas 1994*, vol. 3, *Salinity*, *NOAA Atlas NESDIS 3*, 99 pp., Natl. Oceanic and Atmos. Admin., Silver Spring, Md.
Marcus, S. L., Y. Chao, J. O. Dickey, and P. Gegout (1998), Detection and modeling of nontidal oceanic effects on Earth's rotation rate, *Science*, *281*, 1656–1659.
Marshall, J., C. Hill, L. Perelman, and A. Adcroft (1997a), Hydrostatic, quasi-hydrostatic, and nonhydrostatic ocean modeling, *J. Geophys. Res.*, *102*, 5733–5752.
Marshall, J., A. Adcroft, C. Hill, L. Perelman, and C. Heisey (1997b), A finite-volume, incompressible, Navier Stokes model for studies of the ocean on parallel computers, *J. Geophys. Res.*, *102*, 5753–5766.
Mellor, G. L., and T. Ezer (1995), Sea level variations induced by heating and cooling: An evaluation of the Boussinesq approximation in ocean models, *J. Geophys. Res.*, *100*, 20,565–20,577.
Munk, W. H., and G. J. F. MacDonald (1960), *The Rotation of the Earth: A Geophysical Discussion*, 323 pp., Cambridge Univ. Press, New York.
Naito, I., and N. Kikuchi (1990), A seasonal budget of the Earth's axial angular momentum, *Geophys. Res. Lett.*, *17*, 631–634.
Naito, I., and N. Kikuchi (1991), Reply to Rosen and Salstein's comment, *Geophys. Res. Lett.*, *18*, 1927–1928.
Percival, D. B., and A. T. Walden (1993), *Spectral Analysis for Physical Applications: Multitaper and Conventional Univariate Techniques*, 610 pp., Cambridge Univ. Press, New York.
Philander, S. G. (1990), *El Niño, La Niña, and the Southern Oscillation*, 303 pp., Academic, San Diego, Calif.
Ponsar, S., V. Dehant, R. Holme, D. Jault, A. Pais, and T. Van Hoolst (2003), The core and fluctuations in the Earth's rotation, in *Earth's Core: Dynamics, Structure, Rotation*, *Geodyn. Ser.*, vol. 31, edited by V. Dehant et al., pp. 251–261, AGU, Washington, D. C.
Ponte, R. M. (1993), Variability in a homogenous global ocean forced by barometric pressure, *Dyn. Atmos. Oceans*, *18*, 209–234.
Ponte, R. M. (1994), Understanding the relation between wind- and pressure-driven sea level variability, *J. Geophys. Res.*, *99*, 8033–8039.
Ponte, R. M. (1997), Oceanic excitation of daily to seasonal signals in Earth rotation: Results from a constant-density numerical model, *Geophys. J. Int.*, *130*, 469–474.
Ponte, R. M. (1999), A preliminary model study of the large-scale seasonal cycle in bottom pressure over the global ocean, *J. Geophys. Res.*, *104*, 1289–1300.
Ponte, R. M., and A. H. Ali (2002), Rapid ocean signals in polar motion and length of day, *Geophys. Res. Lett.*, *29*(15), 1711, doi:10.1029/2002GL015312.
Ponte, R. M., and D. Stammer (2000), Global and regional axial ocean angular momentum signals and length-of-day variations (1985–1996), *J. Geophys. Res.*, *105*, 17,161–17,171.
Ponte, R. M., D. Stammer, and C. Wunsch (2001), Improving ocean angular momentum estimates using a model constrained by data, *Geophys. Res. Lett.*, *28*, 1775–1778.
Rosen, R. D. (1993), The axial momentum balance of Earth and its fluid envelope, *Surv. Geophys.*, *14*, 1–29.
Rosen, R. D., and D. A. Salstein (1985), Contribution of stratospheric winds to annual and semi-annual fluctuations in atmospheric angular momentum and the length of day, *J. Geophys. Res.*, *90*, 8033–8041.
Rosen, R. D., and D. A. Salstein (1991), Comment on "A seasonal budget of the Earth's axial angular momentum" by Naito and Kikucho, *Geophys. Res. Lett.*, *18*, 1925–1926.
Salstein, D. A., and R. D. Rosen (1997), Global momentum and energy signals from reanalysis systems, paper presented at 7th Conference on Climate Variations, Am. Meteorol. Soc., Boston, Mass.
Salstein, D. A., D. M. Kann, A. J. Miller, and R. D. Rosen (1993), The Sub-Bureau for Atmospheric Angular Momentum of the International Earth Rotation Service: A meteorological data center with geodetic applications, *Bull. Am. Meteorol. Soc.*, *74*, 67–80.
Segschneider, J., and J. Sündermann (1997), Response of a global circulation model to real-time forcing and implications to Earth's rotation, *J. Phys. Oceanogr.*, *27*, 2370–2380.
Stammer, D., C. Wunsch, I. Fukumori, and J. Marshall (2002), State estimation improves prospects for ocean research, *Eos Trans. AGU*, *83*(27), 289–295.
Wahr, J. M. (1982), The effects of the atmosphere and oceans on the Earth's wobble: I. Theory, *Geophys. J. R. Astron. Soc.*, *70*, 349–372.
Willebrand, J., S. G. H. Philander, and R. C. Pacanowski (1980), The oceanic response to large-scale atmospheric disturbances, *J. Phys. Oceanogr.*, *10*, 411–429.
Wunsch, C., and D. Stammer (1997), Atmospheric loading and the oceanic "inverted barometer" effect, *Rev. Geophys.*, *35*, 79–107.
Yoder, C. F., J. G. Williams, and M. E. Parke (1981), Tidal variations of Earth rotation, *J. Geophys. Res.*, *86*, 881–891.

I. Fukumori, R. S. Gross, and D. Menemenlis, Jet Propulsion Laboratory, California Institute of Technology, 4800 Oak Grove Drive, Pasadena, CA 91109, USA. (if@pacific.jpl.nasa.gov; richard.gross@jpl.nasa.gov; menemenlis@jpl.nasa.gov)

P. Gegout, Institut de Physique du Globe, 5 rue Rene Descartes, Strasbourg F- 67084, France. (pascal.gegout@eost.u-strasbg.fr)